Thermal catalytic etching of diamond by double-metal layers

D.D. Tran, C. Mannequin, M. Bonvalot, A. Traoré, H. Mariette, M. Sasaki, Etienne Gheeraert

Thermal Catalytic Etching of Diamond by Double-Metal Layers

D.D.Tran[a,b,c], C.Mannequin[c,d], M.Bonvalot[c,e], A.Traore[b,c], H.Mariette[a,c], M.Sasaki[b], E.Gheeraert[a,b,c]

[a] *Univ. Grenoble Alpes, CNRS, Grenoble INP, Institut Neel, Grenoble, 38000, France*
[b] *Institute of Applied Physics, Faculty of Pure and Applied Sciences, University of Tsukuba, Tsukuba, 305-8573, Japan*
[c] *Japanese-French lAboratory for Semiconductor physics and Technology J-FAST, CNRS, Université Grenoble Alpes, Grenoble INP, University of Tsukuba, Japan,*
[d] *CNRS-Nantes Universite-Institut des Matériaux de Nantes Jean Rouxel, Nantes cedex 3, 44322, France*
[e] *Univ. Grenoble Alpes, CNRS, LTM, Grenoble, 38000, France*

Abstract

We introduce a novel technique for thermal catalytic etching of single-crystal diamond under hydrogen atmosphere using a double-metal layer consisting of two different metallic thin films. Surface phenomena, catalytic activity, hydrogen pressure dependence and etch rates in several double-metal layer configurations were investigated. We observe that etching with an optimized thickness ratio of Ni/Pd films increases the etch rate by a factor up to 11 compared to etching with a single-metal layer Ni film. The proposed double-metal layer technique enhances hydrogen absorption, which contributes to an increased etch rate of the process, as compared to conventional single-metal layer thermal catalytic etching. Moreover, the etched pattern shows smooth (111) plane sidewalls and flat (100) step-terrace bottom features.

Keywords:
Diamond, Catalytic Etching, Solid solution reaction, Solubility, Anisotropic Etching, Hydrogen

1. Introduction

Diamond has excellent physical and electronic properties such as the highest known thermal conductivity of any material (22 $W.cm^{-1}.K^{-1}$ at room temperature [1]), high hole-electron mobilities ($>$ 1060-2100 $cm^2.V^{-1}.s^{-1}$ [2]), high critical

electric field (9.5 MV.cm^{-1} [3]) and ultra-wide band gap (5.47 eV [1]), making it an excellent candidate for wide range of applications as high-power electronics [4], radiation detectors [5] and photonic devices [6], among others. Advanced diamond devices for such applications require a semi-vertical architecture with the active channel located on the etched sidewalls of the active layer [4]. Precise control of the etched sidewalls is a challenge in directional plasma etching, where anisotropy forms through the preferential movement of reactive particles or by the shape and edges of etching mask. Additionally, plasma etching processes have inherent limitations such as subsurface crystallographic damage caused by ion bombardment, which partially transforms the diamond crystal structure into graphite or amorphous material [7].

Recently, thermal catalytic etching (TCE) has emerged as a robust anisotropic process promising for the fabrication of diamond-based 3D devices [8] [9] [10] [11] [12] [13] [14] [15] [16] [17] [18] [19]. It is based on the catalytic reaction of diamond with various transition metals at high temperature under reactive gas atmospheres such as hydrogen. These metal catalysts reduce the energy barrier of diamond etching by breaking bonds between carbon atoms to dissolve them near the metal-diamond interface [20].

In the TCE process, a thin film of a metallic catalyst is directly deposited on the diamond surface. The sample is then heated under a hydrogen atmosphere. At high temperature, carbon atoms at the metal-diamond interface are gradually dissolved into the metal film. Simultaneously, hydrogen is absorbed and diffuse into the metallic matrix, where both carbon and hydrogen atoms react and form methane as a by-product, which desorbs from the metal surface. As the process continues, carbon atoms under the metal film are gradually removed [8].

Due to its crystalline structure, diamond preferentially breaks along cleavage planes with lower cohesion energies, which unveils the (111) plane due to its high atomic density [20]. Accordingly, TCE of (100) diamond substrates results in patterns with tilted atomically flat sidewalls corresponding to (111) planes, whereas the bottom of the etched feature remains as (100) plane. Therefore the anisotropy in the TCE process is due to the intrinsic properties of monocrystalline diamond and not to the etching process itself, as in plasma etching. Thermal catalytic etching of diamond using a single-metal layer (SML) of nickel under hydrogen atmosphere [17] [18] has been reported. An etch rate of 0.6-0.75 μm.h^{-1} was reported for TCE of single-crystal diamond using a 200 nm thin nickel film under a hydrogen pressure as high as 375 Torr [18]. However, the etchings require high hydrogen pressure conditions.

The etch rate obtained in a diamond TCE depends on both the hydrogen flux

into the metal surface and the flux of dissolved carbon formed from the diamond-metal interface. Therefore, a metal with high carbon and hydrogen solubility is required to achieve a high etch rate. Ni and Fe both have high carbon solubility at high temperature (930 °C) but limited hydrogen solubility, see Figure 1, making the etching process ineffective. In contrast, Pd and Zr exhibit high hydrogen solubility but extremely low carbon solubility, which in turn prevents effective diamond etching. Ti gives an acceptable compromise for TCE of diamond due to its relatively high solubility for both carbon and hydrogen. However, the formation of highly stable titanium carbide TiC at the metal-diamond interface at high temperature make it unusable for diamond TCE [21]. Therefore, diamond etching is limited when using SML.

In this work, we present for the first time an approach based on a double-metal layer (DML) for TCE of diamond, which significantly improves the observed etch rate. In stead of using a SML for etching, we utilize a layer composed of two different metal films. The metal at the interface with diamond (interface-metal) exhibits a high carbon solubility to enhance the carbon dissolution process, while the metal on the surface (surface-metal) has a high hydrogen solubility to promote hydrogen absorption.

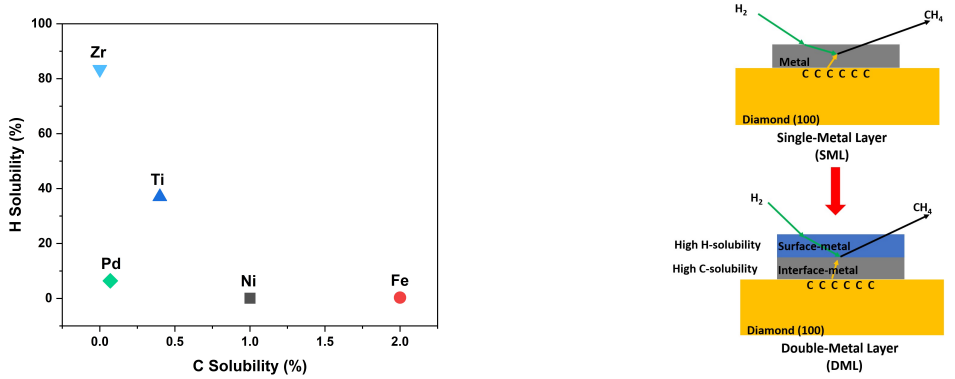

(a) (b)

Figure 1: (a): Hydrogen and carbon solubility (% in atom fraction) of commonly used catalyst metals at a temperature around 930 °C. The values are estimated from [22] for hydrogen and [23] and [24] for carbon. (b): Double-metal layer (DML) approach in which a single-metal layer (SML) catalyst is replaced by a film containing two metal layers: interface-metal with high C solubility and surface-metal with high H solubility.

Solubility data from Figure 1 suggests that both Ni and Fe are reasonable

choices as the interface-metal in contact with diamond. However, Fe has been reported to form a chemically stable carbide at temperatures above 527 °C (930 K) [25], which is difficult to remove even in hot, acidic cleaning solutions. In contrast, Ni does not form a carbide material at any temperature [25]. Furthermore, Ni and cubic diamond have the same fcc crystal structure with a very low lattice mismatch (0.35 nm for Ni lattice parameter versus 0.36 nm for diamond), which can result in a thermally stable Ni-diamond interface. For these reasons, Ni is selected as the interface-metal which is directly deposited on the diamond surface in the DML catalyst system. Both Zr and Pd are used for surface-metal due to their high hydrogen solubility.

Table 1: Physical and thermal properties of Ni, Zr, Pd. The solubilities are estimated at temperature about 930°C from [22] for hydrogen; [23] and [24] for carbon.

Metal	Crystal structure	Lattice parameter (nm)	Expansion coefficient (ppm)	Melting point (°C)	C solubility %	H solubility %
Ni	fcc	0.35, 0.35, 0.35	13.1	1455	1 [23]	0.09 [22]
Pd	fcc	0.38, 0.38, 0.38	11.76	1555	0.07 [23]	6.4 [22]
Zr	hcp	0.32, 0.32, 0.5	5.85	1855	0 [24]	83 [22]

First, we investigate Ni/Zr and Ni/Pd DMLs with different thickness ratios to determine the optimized configuration. The etch rate, physical and chemical phenomena that occur on the DML surface are discussed. As a reference, etching with Ni SML is also studied. Secondly, the dependence of the etch rate on the hydrogen pressure is investigated. Finally, the morphology of the etched pattern is presented.

2. Material and Methods

Chemical vapor deposition (CVD) single-crystal diamond substrates with a (100) surface orientation are first immersed in a tri-acid solution ($HClO_4$: HNO_3: H_2SO_4 in a molar ratio of 1:3:4) at 250 °C to remove organic and mineral contaminants from the surface. Metallic patterns are obtained by lift-off after resist patterning by Smartprint photolithography followed by metallic film deposition (Ni, Zr, Pd) by electron-beam evaporation. Ni is chosen as the interface-metal, and the Pd and Zr films used as the surface-metal are deposited immediately after the formation of the Ni layer to prevent any contamination at the metal-metal interface.

Etching experiments are carried out in a CVD reactor dedicated to diamond growth at temperature about 930 °C and under a hydrogen flow of 100 sccm at a

Table 2: Conditions for two set of experiments: Metal identity and thickness; and Dependence of hydrogen pressure on etch rate.

Experiment	Metal configuration	Interface-metal (Ni) thickness (nm)	Surface-metal (Zr or Pd) thickness (nm)	H_2 pressure (Torr)	Temperature (°C)	Etching Time (min)
Metal identity and thickness	Ni	260	0	105	930	30
	Ni/Zr	10	250	105	930	30
	Ni/Zr	250	10	105	930	30
	Ni/Pd	10	250	105	930	30
	Ni/Pd	250	10	105	930	30
Hydrogen pressure	Ni	300	0	65	930	30
	Ni	300	0	105	930	30
	Ni/Zr	285	15	65	930	30
	Ni/Zr	285	15	105	930	30
	Ni/Pd	285	15	65	930	30
	Ni/Pd	285	15	105	930	30

pressure of 65 or 105 Torr. Finally, the samples are cooled to room temperature under a stream of hydrogen for 30 minutes. After etching, the metallic surface is observed by scanning electron microscopy (SEM Zeiss Ultra) in both in-lens secondary electron (SE-InLens) and backscattering electron (BSE) modes before being completely removed by a hot bath of aqua regia solution (HNO_3 : HCl in a molar ratio of 1:3, 200 °C, 1 h).

The etched diamond surfaces are then observed by using a SEM. The etch depth is measured by using an optical profiler (ContourGT) by determining the difference between the average vertical attitude Z-measurement of the etched pattern bottom and the average vertical attitude Z-measurement of the pattern borders.

The TCE of diamond by DML is systematically examined using the two metal pairs Ni/Zr and Ni/Pd. The experimental details are listed in Table 2.

In a first series of experiments, two DML thickness configurations are tested: thin interface-metal layer with thick surface-metal layer: 10Ni/250Zr (film contains of 10 nm of Ni and 250 nm of Zr on top) and 10Ni/250Pd; thick interface-metal layer with thin surface-metal layer: 250Ni/10Zr and 250Ni/10Pd. The experimental results obtained in these two configurations are systematically compared with those obtained with the TCE of diamond using a 260Ni SML, which is our reference configuration. The etching is performed at 930 °C for 30 minutes under a hydrogen atmosphere of 105 Torr. To explain these results, metallic surfaces after etching are observed by SEM. To examine the effect of hydrogen pressure, diamond was etched with: 300Ni SML, 285Ni/15Zr DML and 285Ni/15Pd DML under 65 Torr and 105 Torr hydrogen pressures.

3. Results and Discussion

3.1. Metal identity and thickness

Figure 2 shows the etch rates of different metal thickness configurations in the DML approach. Using the etch rate obtained for the SML standard as the basis for comparison, the etch rates of 10Ni/250Zr DML and 10Ni/250Pd DML are low, with the 10Ni/250Zr sample showing no detectable etching. Using 250Ni/10Zr DML slightly reduces the etch rate compared to 260Ni SML, while using 250Ni/10Pd DML triples the etch rate. SEM observations of the metal films after etching are summarized in Table 3.

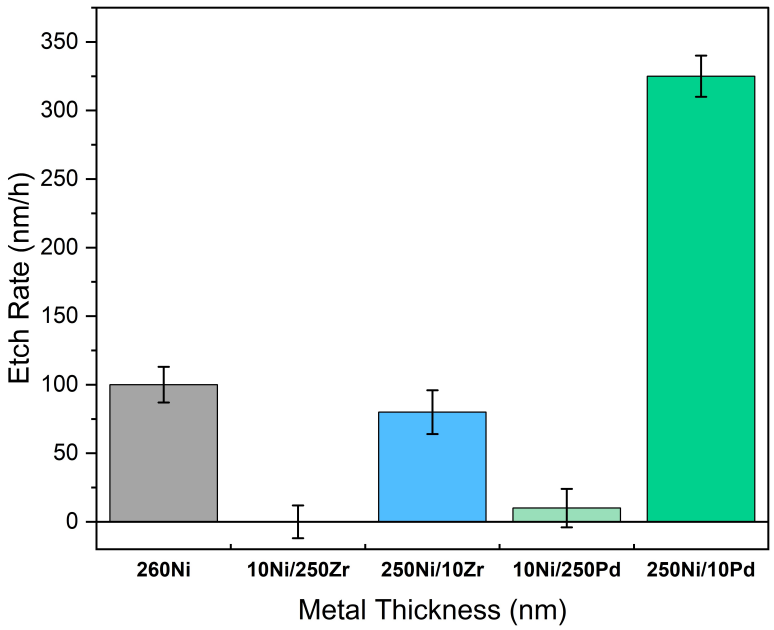

Figure 2: Etch rate of thermal catalytic etching of diamond with two double-metal layer configurations: 10nmNi/250nmZr, 10nmNi/250nmPd and 250nmNi/10nmZr, 250nmNi/10nmPd. Etching by single-metal layer of 260nmNi as reference. Etching condition: 930 °C, 105 Torr H_2, 30 minutes.

Table 3: Summary of metal film behavior after etching.

	Etch Rate $nm.h^{-1}$	SEM images observation of metal surface	Surface phenomena
SML-260Ni	100	Several dark spots on a grey color surface	Ni film saturated with carbon, carbon accumulates on the outer surface.
DML-10Ni/250Zr	0	Homogeneous grey color surface	The thick Zr film blocks carbon flow to the outer surface. There is no carbon accumulation on the outer surface.
DML-250Ni/10Zr	80	Several dark spots on a grey color surface	The Ni film is saturated with carbon, the Zr thin film is eventually broken thus shows carbon accumulation sites.
DML-10Ni/250Pd	10	Several grey spots on a dark surface	Dewetting of the Ni/Pd film creates micro metallic particles on the diamond surface.
DML-250Ni/10Pd	325	Several dark spots on a grey surface	Thin Pd film dissolved in Ni forms a solid Pd-Ni solution. Carbon accumulates in several places on the outer surface.

3.1.1. Etching with Ni single-metal layer

Figure 3 shows SEM images of the 260Ni SML surface after etching: the SE-InLens image (Figure 3a) shows state of the metal surface. The higher magnification of BSE images (Figure 3b) shows the element distribution: grey areas

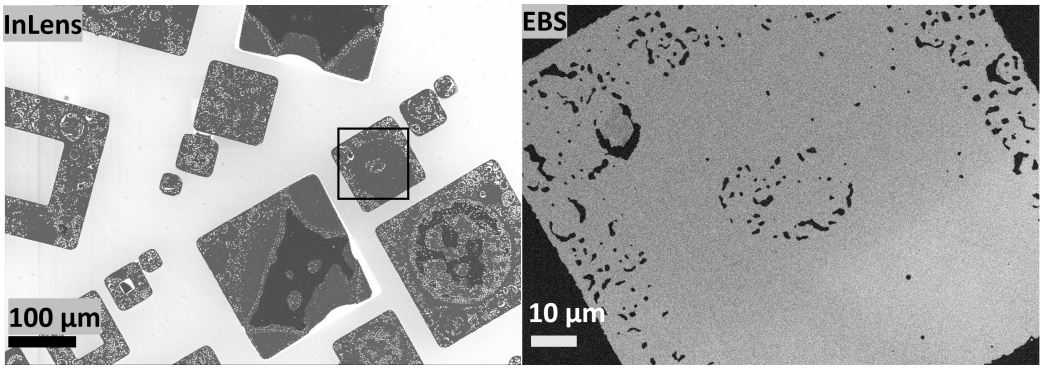

(a) (b)

Figure 3: SEM images after etching with 260nmNi single-metal layer surface: SE-InLens image (a) and its higher magnification BSE image (b). Etching conditions: 930 °C, 105 Torr H_2, 30 minutes.

correspond to Ni (heavier atomic mass), while dark spots indicate the presence of carbon at the surface. The presence of carbon as well as the relatively low etch rate in the reference sample confirms the ineffective hydrogen absorption in Ni SML. During the etching process, carbon is gradually dissolved and then continuously diffuses to the outer surface. However, due to a low concentration of absorbed hydrogen, there is less methane formation, leading to supersaturation of the Ni surface with carbon. For continuous methane formation, the metal surface must maintain contact with hydrogen gas to produce atomic hydrogen through dissociation. Therefore, these carbon accumulation areas as shown in the image can lead to deactivation of the catalyst as reported in [8]. Consequently, the etch rate with Ni SML is low.

3.1.2. Etching with Ni/Zr double-metal layer

Figure 4a suggests that the 10Ni/250Zr DML surface after etching appears homogeneously grey in color, indicating no carbon accumulation on the outer surface. This could be explained by the Ni layer being too thin to initiate carbon dissolution. In addition, the thick Zr layer with low carbon solubility could inhibit any possible carbon or methane diffusion to the surface. As a result, no carbon was detected on the metal surface and no etching is observed.

BSE-SEM images of 250Ni/10Zr DML after etching are shown in Figure 4b. A grey background with several dark spots is observed, suggesting that there is some carbon accumulation on the outer surface. Thin films deposited with an

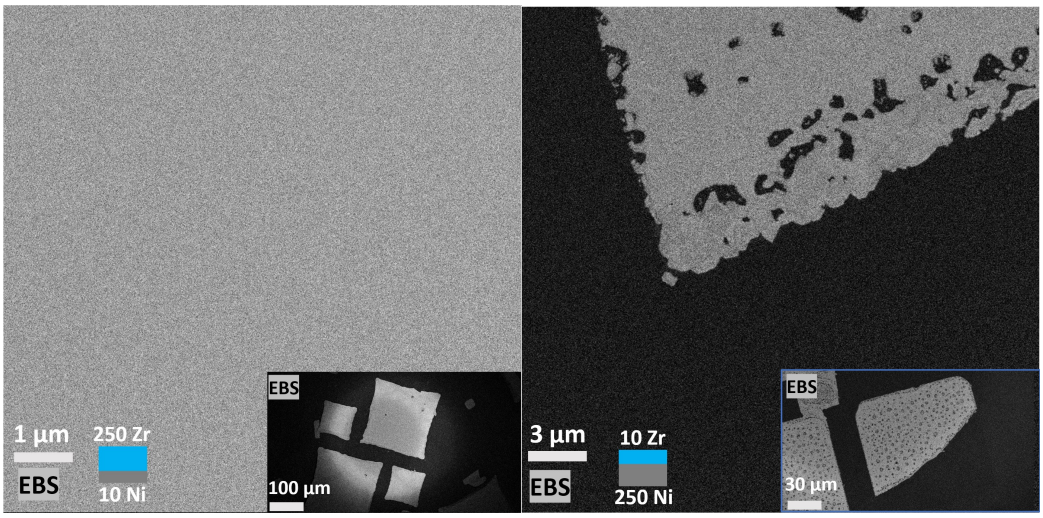

(a) (b)

Figure 4: SEM BSE images after etching with Ni/Zr double-metal layers: (a)10nmNi/250nmZr, (b)250nmNi/10nm Zr. Inserts show the samples at low magnification. Etching conditions: 930 °C, 105 Torr H_2, 30 minutes.

electron beam evaporator can have a polycrystalline structure. The change from the fcc crystal structure of Ni to the hcp structure of Zr, as shown in Table 1, results in a mismatch at the Ni-Zr interface. Furthermore, the solubility of Zr in Ni at 930 °C estimated from the alloy phase diagram [24] is low with a concentration of about 2%. Therefore, the discontinuous Ni-Zr interface can prevent the diffusion and reaction between carbon dissolved at the Ni-diamond interface and the atomic hydrogen absorbed by the Zr layer. Thus, the Ni thin film became supersaturated, and carbon breaks the Zr thin film at some defect points or grain boundaries. As a result, carbon accumulates on the surface and the etch rate is not significantly improved compared to using an Ni SML film. Although Zr is one of the materials with the highest hydrogen solubility (83% concentration), its discontinuous Ni-Zr interface could render the etching processes ineffective and therefore lead to a low etch rate.

3.1.3. Etching with Ni/Pd double-metal layer

For Ni/Pd DML systems, Figure 5a shows the surface of the 10Ni/250Pd DML after etching. The metal film is completely dewetted and forms microparticles (grey color) on the diamond surface (dark color). In a gas environment, the de-

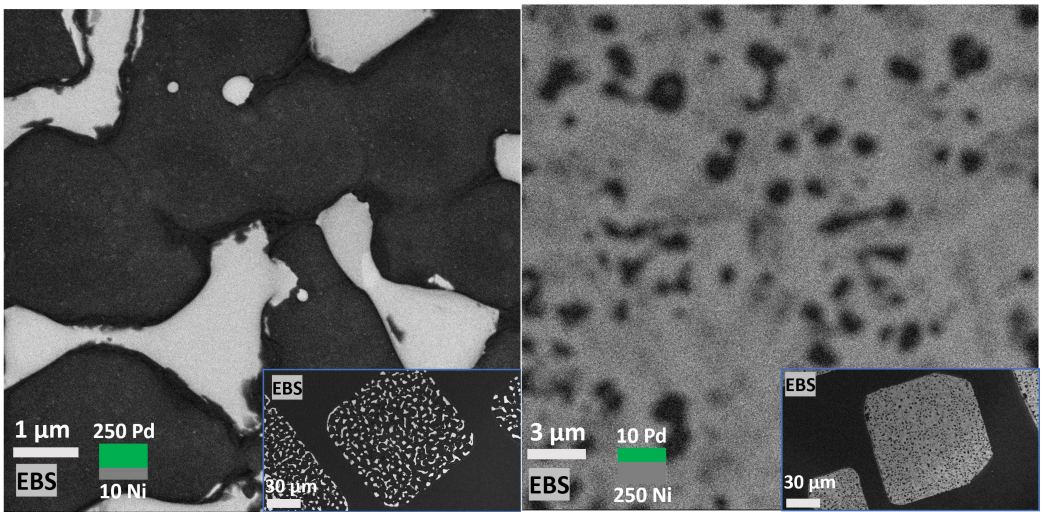

(a) (b)

Figure 5: SEM BSE images after etching with Ni/Pd double-metal layers: (a) 10nmNi/250nmPd, (b) 250nmNi/10nmPd. Inserts show the samples at low magnification. Etching conditions: 930 °C, 105 Torr H_2, 30 minutes.

creasing melting temperature of the metal on the diamond surface has been reported [25]. The phenomenon of lowering the melting temperature of metals upon absorption of hydrogen has been explained [26] as a consequence of the increased number of sites for hydrogen atoms in the liquid state compared to the solid state. In the case of 10Ni/250Pd DML, the melting point of Pd (1555 °C) is much lower than that of Zr (1855 °C), see Table 1. As a result, 10Ni/250Pd DML is dewetted into microparticles at high-temperature under hydrogen atmosphere, while 10Ni/250Zr DML is not dewetted (Figure 4a). The micro/nanoparticles formed containing Pd, Ni or a Ni-Pd solid solution, can etch the diamond surface. TCE of diamond by Ni nanoparticles has been reported [11]. The etch rate by Ni particules is relatively small.

Finally, Figure 5b shows the surface of 250Ni/10Pd DML after etching. The metal surface (grey color) is inhomogeneous and covered by carbon accumulations (dark spots). Pd and Ni have similar crystal structure, lattice parameter, expansion coefficient and melting point, see Table 1. In addition, the phase diagram of Ni-Pd alloy [24] shows that Pd completely dissolves into Ni at high temperature. Thus, a thin Pd layer could form a solid solution with Ni. The solubility of a gas in a solid solution alloy depends more on the metal having a higher

solubility [27]. At 930 °C, the hydrogen solubility for Ni is about 0.09% and for Pd is up to 6.4%. Therefore, the Ni-Pd surface has a much higher hydrogen concentration adsorption than an Ni SML surface.A similar effect has been reported for the reduction of the hydrogen dissociation energy of the Pd-doped Ni cluster [28]. The hydrogen dissociation energy decreases from -2 eV for Ni clusters to -3.2 eV for Pd-doped Ni clusters indicating the hydrogen dissociation process is more effective in the Ni/Pd system. The lowered dissociation barrier of Ni/Pd DMLs and a higher hydrogen concentration in the latter lead to increase the rate of methane formation. Therefore, the etch rate is improved by a factor of 3 compared to etching with SML Ni. This mechanism is shown in Figure 6.

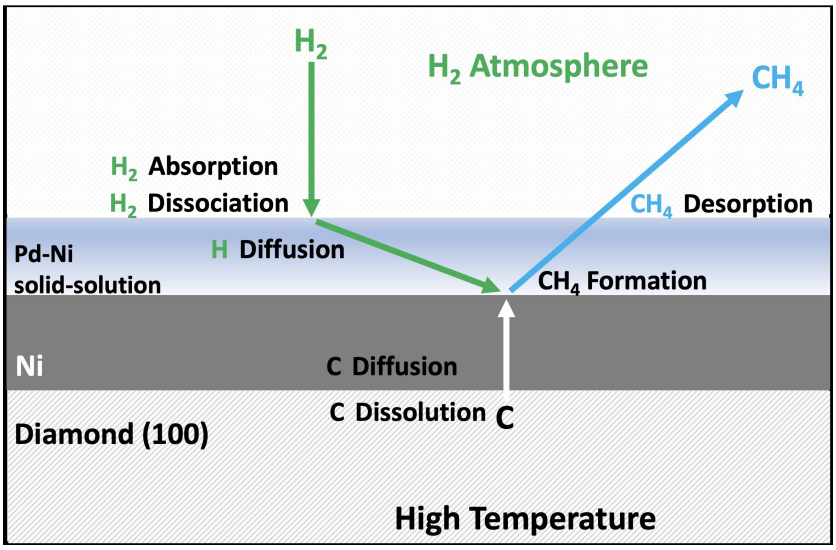

Figure 6: : Mechanism of thermal catalytic etching of diamond by Ni/Pd double-metal layer.

3.2. Impact of hydrogen pressure

Figure 7 shows that when the hydrogen pressure increases from 65 Torr to 105 Torr, the etch rate increases three times for Ni and Ni/Pd films, while it does not change for Ni/Zr film. It is found that the Ni/Pd DML improves the etch rate by 11 times at 65 Torr and almost 9 times at 105 Torr compared to the Ni SML, showing a strong improvement of etching by the DML approach.

The etch rate with a Ni/Zr DML does not significantly change with increasing hydrogen pressure. The rate limiting step in the case of the Ni/Zr samples is the dissolution and diffusion of carbon to the reaction interface as explained in Section

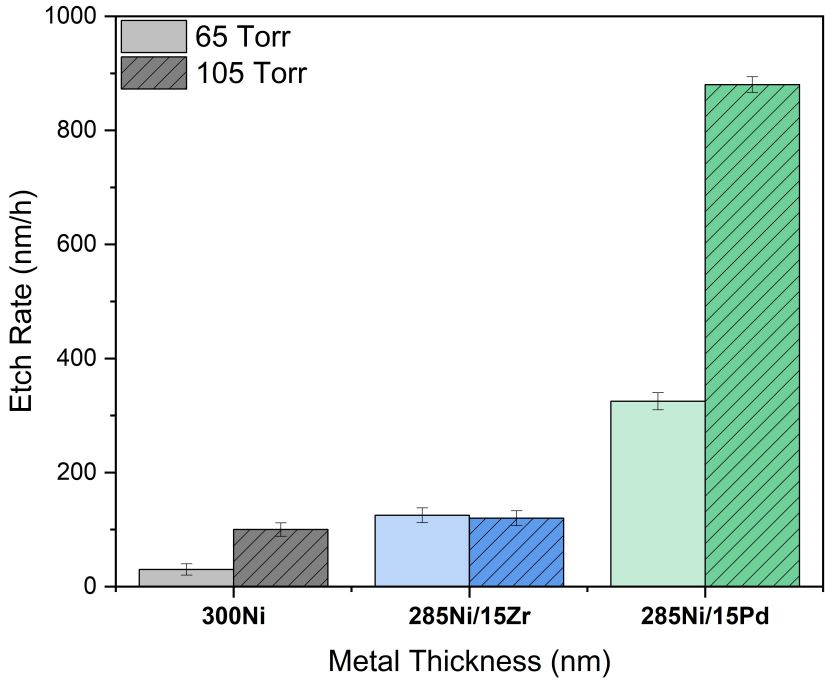

Figure 7: Etch rate of thermal catalytic etching of diamond with: single-metal layer 300nmNi ; double-metal layer 285nmNi/15nmZr; double-metal layer 285nmNi/15nmPd, under 65 Torr and 105 Torr H_2 at 930 °C for 30 minutes.

3.1.2. Thus, increasing the hydrogen pressure is expected to provide no additional benefit to the reaction and the etch rate remains unchanged.

When etching with Ni SML and Ni/Pd DML, the etch rates increase with increasing pressure due to increasing hydrogen solubility. Sievert's laws describe that the solubility S of a gas in the metal increases with the square root of the pressure, so that a square root dependence of the etch rate on the pressure is to be expected [29]. However, the etch rates increase by a factor 3: from 30 $nm.h^{-1}$ to 100 $nm.h^{-1}$ for etching with Ni SML and from 325 $nm.h^{-1}$ to 880 $nm.h^{-1}$ for etching with Ni/Pd DML when the pressure is increased from 65 Torr to 105 Torr. The change in etch rate is larger than expected. It has been reported that the experimental dependence of hydrogen solubility in Pd is in excess of the square root

relation [29]. Sieverts law is accurate at high pressure conditions where the metal surface is saturated by gas molecules. At low pressure, the amount of adsorbed gas is much lower than uni-molecular layer. Thus dependence of solubility S on pressure P can be written as: $S \propto \sqrt{P}.\vartheta \propto \sqrt{P}.aP/(aP + 1)$, where ϑ stands for fraction of the surface covered and a is a constant for a gas-metal system [29]. At the low pressure limit where $aP \ll 1$, the dependence becomes $S \propto P^{1.5}$. Therefore, when hydrogen pressure changed from 65 Torr to 105 Torr and the etch rate by Ni/Pd film increased from 325 $nm.h^{-1}$ to 880 $nm.h^{-1}$.

Note that when etching at 105 Torr, the etch rate of 300Ni SML (100 $nm.h^{-1}$) is the same as 260Ni SML (100 $nm.h^{-1}$), while the etch rate of 285Ni/15Pd DML (880 $nm.h^{-1}$) is about three times that of 250Ni/10Pd DML (325 $nm.h^{-1}$), see Figures 2 and Figure 7. These results show that the etch rate is limited by the hydrogen absorption from the surface and not by the carbon dissolved from the diamond-metal interface. In addition, it can be assumed that at high temperature, the diffusion of hydrogen in thin films is fast enough, so the etch rate directly depends on the amount of hydrogen absorption. In the Ni/Pd DML approach, the amount of hydrogen absorption is determined by the thickness of the Ni-Pd solid-solution layer. The results of etching with 250Ni/10Pd and 285Ni/15Pd DML confirm that a thicker Pd layer gives a higher etch rate.

In comparision to [18]: TCE with 200Ni SML under 375 Torr H_2, with etch rate of 750 nm/h; the etching with a 285nmNi/15nmPd DML gives a higher etch rate, 880 nm/h, for etching under a much lower hydrogen pressure, 105 Torr. Since the etching rate increases sharply as the hydrogen pressure increases, we assume that when etching with a Ni/Pd DML at 375 Torr H_2, the etch rate is well above 880 nm/h.

3.3. Surface morphology of etched pattern by Ni Pd layer

Figure 8 shows the morphology of the etched patterns after etching with Ni/Pd film under 65 Torr at 930 °C for 30 minutes after removing of the catalytic DML. The sidewalls reveal a very smooth (111) surface. The etched bottom has a step-terrace structure. Similar step-terrace structure has been observed and described as an atomically flat diamond (100) surface formation due to anisotropic etching resulting from the solid solution reaction of carbon with Ni [13]. Note that the diamond surface without catalytic metal deposition exhibits square patterns due to atomic hydrogen-induced corrosion during the experiment, which can be limited by optimizing the process.

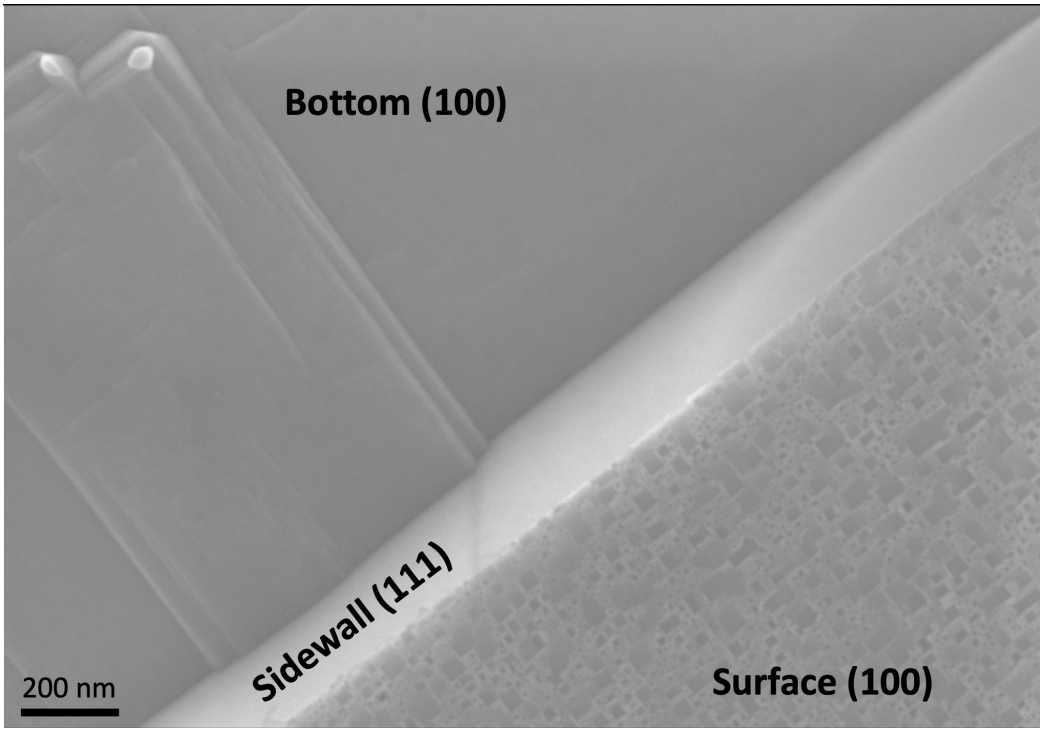

Figure 8: SEM SE image of the diamond surface after etching with a 285nmNi/15nmPd double-metal layer (65 Torr hydrogen, 930 °C).

4. Conclusion

The Ni/Pd double-metal layer significantly improves the etch rate in thermal catalytic etching of single crystal diamond at high-temperature under hydrogen atmosphere. Etching with Ni single-metal layers is slow due to low hydrogen solubility in Ni. Etching with a Ni/Zr double-metal layer does not improve the process because the different crystal structure, lattice mismatch and their thermal properties resulting in a discontinuous Ni-Zr interface that blocks carbon and hydrogen diffusion. A double-metal layer with a thick Ni interface layer and a thin Pd surface layer showed the best results. This was attributed to the thin Pd layer forming a solid solution with Ni at high temperature to improve both the solubility and dissociation of hydrogen, creating a continuous Ni/Pd boundary where carbon and hydrogen easily can react. Therefore, the etch rate with a 285nmNi/15nmPd double-metal layer at 65 Torr H_2 is 11 times higher than etch rate with a 300nmNi single-metal and is 9 times higher at 105 Torr H_2. When the pressure increases

from 65 Torr to 105 Torr, the etch rate of the 285nmNi/15nmPd double metal layer increases three times, indicating that at low pressure, the dependence of hydrogen solubility on pressure exceeds the square root relationship in Sievert's law. A pattern with smooth (111) sidewall and flat step terrace (100) was observed. The high etch rate, high quality of sidewalls and bottom achieved in thermal catalytic etching by the double-layer technique are promising for the fabrication of diamond electronic devices, especially for semi-vertical architectural designs. The result opens possibilities for the use of dual catalyst layers in catalytic etching of materials and other catalyst applications where multiple conditions (at the material-catalyst interface, the catalyst-gas surface, etc...) are required.

Acknowledgment

This work was funded by IDEX ISP 2020-l'initiative d'excellence (Idex) Université Grenoble Alpes and supported by IDEX mobility grant. The author would like to thank Arnaud Claudel from Institute NEEL and colleagues from the start-up DiamFab for technical formations, supports and scientific advice for this work.

References

[1] H. Umezawa, Recent advances in diamond power semiconductor devices, Materials Science in Semiconductor Processing 78 (2018) 147–156.

[2] S. Koizumi, H. Umezawa, J. Pernot, M. Suzuki, Power electronics device applications of diamond semiconductors, Woodhead publishing, 2018.

[3] P.-N. Volpe, P. Muret, J. Pernot, F. Omnes, T. Teraji, F. Jomard, D. Planson, P. Brosselard, N. Dheilly, B. Vergne, et al., High breakdown voltage schottky diodes synthesized on p-type cvd diamond layer, physica status solidi (a) 207 (9) (2010) 2088–2092.

[4] N. Donato, N. Rouger, J. Pernot, G. Longobardi, F. Udrea, Diamond power devices: state of the art, modelling, figures of merit and future perspective, Journal of Physics D: Applied Physics 53 (9) (2019) 093001.

[5] M. Pomorski, B. Caylar, P. Bergonzo, Super-thin single crystal diamond membrane radiation detectors, Applied physics letters 103 (11) (2013).

[6] S. Mi, M. Kiss, T. Graziosi, N. Quack, Integrated photonic devices in single crystal diamond, Journal of Physics: Photonics 2 (4) (2020) 042001.

[7] Y. Kawabata, J. Taniguchi, I. Miyamoto, Xps studies on damage evaluation of single-crystal diamond chips processed with ion beam etching and reactive ion beam assisted chemical etching, Diamond and related materials 13 (1) (2004) 93–98.

[8] V. Ralchenko, T. Kononenko, S. Pimenov, N. Chernenko, E. Loubnin, V. Y. Armeyev, A. Y. Zlobin, Catalytic interaction of fe, ni and pt with diamond films: patterning applications, Diamond and Related Materials 2 (5-7) (1993) 904–909.

[9] A. Chepurov, V. Sonin, J.-M. Dereppe, The channeling action of iron particles in the catalyzed hydrogenation of synthetic diamond, Diamond and related materials 9 (8) (2000) 1435–1438.

[10] T. Ohashi, W. Sugimoto, Y. Takasu, Catalytic etching of $\{100\}$-oriented diamond coating with fe, co, ni, and pt nanoparticles under hydrogen, Diamond and related materials 20 (8) (2011) 1165–1170.

[11] H.-A. Mehedi, J.-C. Arnault, D. Eon, C. Hébert, D. Carole, F. Omnes, E. Gheeraert, Etching mechanism of diamond by ni nanoparticles for fabrication of nanopores, Carbon 59 (2013) 448–456.

[12] J. Wang, L. Wan, J. Chen, J. Yan, Anisotropy of synthetic diamond in catalytic etching using iron powder, Applied Surface Science 346 (2015) 388–393.

[13] K. Nakanishi, H. Kuroshima, T. Matsumoto, T. Inokuma, N. Tokuda, Atomically flat diamond (100) surface formation by anisotropic etching of solid-solution reaction of carbon into nickel, Diamond and Related Materials 68 (2016) 127–130.

[14] K. Liu, Z. Lv, B. Dai, G. Shu, J. Zhao, B. Liu, W. Wang, J. Xue, K. Yao, M. Sun, et al., High-selectivity anisotropic etching of single-crystal diamond by h plasma using iron catalysis, Diamond and Related Materials 86 (2018) 186–192.

[15] M. Nagai, K. Nakanishi, H. Takahashi, H. Kato, T. Makino, S. Yamasaki, T. Matsumoto, T. Inokuma, N. Tokuda, Anisotropic diamond etching through thermochemical reaction between ni and diamond in high-temperature water vapour, Scientific reports 8 (1) (2018) 6687.

[16] M. Nagai, Y. Nakamura, T. Yamada, T. Tabakoya, T. Matsumoto, T. Inokuma, C. E. Nebel, T. Makino, S. Yamasaki, N. Tokuda, Formation of u-shaped diamond trenches with vertical $\{111\}$ sidewalls by anisotropic etching of diamond (110) surfaces, Diamond and Related Materials 103 (2020) 107713.

[17] K. Koyama, S.-W. Kim, M. Yoshimoto, Influence of diamond-etching conditions on the fabrication of diamond microneedles by a thermochemical reaction of ni in an h2 atmosphere, Journal of the Ceramic Society of Japan 129 (7) (2021) 481–484.

[18] C. Schreyvogel, S. Temgoua, C. Giese, V. Cimalla, J. Barjon, C. E. Nebel, Fabrication of n-type doped v-shaped structures on (100) diamond, physica status solidi (a) 218 (7) (2021) 2000502.

[19] Y. Li, Y. Kim, P. V. Bakharev, W. K. Seong, C. Hyun, D. C. Camacho-Mojica, L. Zhang, B. V. Cunning, T. J. Shin, G. Lee, et al., Dissolving diamond: Kinetics of the dissolution of (100) and (110) single crystals in nickel and cobalt films, Chemistry of Materials 34 (6) (2022) 2599–2611.

[20] H. O. Pierson, Handbook of carbon, graphite, diamonds and fullerenes: processing, properties and applications, William Andrew, 2012.

[21] Q. Du, X. Wang, S. Zhang, W. Long, L. Zhang, Y. Jiu, C. Yang, Y. Zhang, J. Yang, Research status on surface metallization of diamond, Materials Research Express 6 (12) (2020) 122005.

[22] T. Chernyayeva, A. Ostapov, Hydrogen in zirconium. part 1, Voprosy Atomnoj Nauki i Tekhniki (2013) 16–32.

[23] H. Yokoyama, H. Numakura, M. Koiwa, The solubility and diffusion of carbon in palladium, Acta materialia 46 (8) (1998) 2823–2830.

[24] H. Baker, H. Okamoto, ASM Handbook, Volume 03 - Alloy Phase Diagrams, ASM International.

[25] Y. Morofushi, H. Matsushita, N. Miki, Microscale patterning of single crystal diamond by thermochemical reaction between sidero-metal and diamond, Precision engineering 35 (3) (2011) 490–495.

[26] Y. Fukai, The metal-hydrogen system: basic bulk properties, Vol. 21, Springer Science & Business Media, 2006.

[27] V. Kiselev, O. Krylov, Adsorption and catalysis of transition metals and their oxides, Indian Journal of Physics 67 201–206.

[28] N. S. Venkataramanan, A. Suvitha, H. Mizuseki, Y. Kawazoe, A theoretical study of the effects of transition metal dopants on the adsorption and dissociation of hydrogen on nickel clusters, International Journal of Quantum Chemistry 113 (15) (2013) 1940–1948.

[29] C. J. Smithells, C. Ransley, The diffusion of gases through metals, Proceedings of the Royal Society of London. Series A-Mathematical and Physical Sciences 150 (869) (1935) 172–197.